Published in final edited form as:
Stem Cells. 2010 October ; 28(10): 1751–1759. doi:10.1002/stem.496.

B-Myb is Critical for Proper DNA Duplication During an Unperturbed S Phase in Mouse Embryonic Stem Cells

Maëlle Lorvellec[a], **Stéphanie Dumon**[a], **Apolinar Maya-Mendoza**[b], **Dean Jackson**[c], **Jon Frampton**[a], and **Paloma García**[a]

[a]Institute of Biomedical Research, College of Medical and Dental Sciences, University of Birmingham, Edgbaston, Birmingham, United Kingdom

[b]Institute of Human Genetics, CNRS, Montpellier, France

[c]Faculty of Life Science, Manchester Interdisciplinary Biocentre, Manchester, United Kingdom

Abstract

A common feature of early embryo cells from the inner cell mass (ICM) and of ESCs is an absolute dependence on an atypical cell cycle in which the G1 phase is shortened to preserve their self-renewing and pluripotent nature. The transcription factor B-Myb has been attributed a role in proliferation, in particular during the G2/M phases of the cell cycle. Intriguingly, B-Myb levels in ICM/ESCs are greater than 100 times compared with those in normal proliferating cells, suggesting a particularly important function for this transcription factor in pluripotent stem cells. B-Myb is essential for embryo development beyond the preimplantation stage, but its role in ICM/ESCs remains unclear. Using a combination of mouse genetics, single DNA fiber analyses and high-resolution three-dimensional (3D) imaging, we demonstrate that B-Myb has no influence on the expression of pluripotency factors, but instead B-Myb ablation leads to stalling of replication forks and superactivation of replication factories that result in disorganization of the replication program and an increase in double-strand breaks. These effects are partly due to aberrant transcriptional regulation of cell cycle proliferation factors, namely c-Myc and FoxM1, which dictate normal S phase progression. We conclude that B-Myb acts crucially during the S phase in ESCs by facilitating proper progression of replication, thereby protecting the cells from genomic damage. Our findings have particular relevance in the light of the potential therapeutic application of ESCs and the need to maintain their genomic integrity.

Correspondence: Paloma García, PhD, Institute of Biomedical Research, College of Medical and Dental Sciences, University of Birmingham, Edgbaston, Birmingham B15 2TT, U.K. Telephone: 44-0-121-414-6807; Fax: 44-0-121-415-8817; p.garcia@bham.ac.uk.

Author contributions: M.L.: collection and/or assembly of the data, data analysis and interpretation, manuscript writing; S.D.: collection of the data; A.M.: technical advice; D.J.: theoretical and technical advice; J.F.: conception and design, final approval of manuscript and financial support; P.G.: conception and design; collection and/or assembly of the data, data analysis and interpretation, manuscript writing, final approval of manuscript and financial support.

Disclosure of Potential Conflicts of Interest: The authors indicate no potential conflicts of interest.

Europe PMC Funders Author Manuscripts

Keywords

Cell cycle; Cell proliferation; Embryonic stem cells; Cancer; Chromosomal aberrations; Cre-loxP system; Conditional knockout

Introduction

Pluripotent ESCs are characterized by their ability to perpetuate indefinitely in vitro and differentiate into all three embryonic germ layers. This is achieved through tight molecular regulatory mechanisms involving the combined action of factors responsible for the maintenance of the pluripotent state and the enforcement of an atypical cell cycle in which the G1 phase is shortened to escape differentiation signals present at this stage [1]. Failure to control these mechanisms in vivo can lead to early embryonic lethality due to inefficient formation of the inner cell mass (ICM). Such lethality has been associated with proteins related to the control of S phase progression, including Cdc7 (MGI:1309511) [2], Mat-1 (MGI:106207) [3], Cdc45 (MGI:1338073), [4] the ATM- and Rad3-related protein kinase (ATR) (MGI: 108028) [5], and Chk1 (MGI:1202 065; MGI:101785) [6].

For many years, B-Myb (MGI:101785) has been recognized as a key transcription factor in the regulation of the cell cycle in somatic cells, and has also been implicated in different types of human cancer [7]. More recently, it has been associated with the maintenance of genome stability through the regulation of genes related to G2/M transition [8-12]. B-Myb is ubiquitously expressed, but its transcript is 100–1,000 times more abundant in ESCs, embryonic germ cells, and embryonic carcinoma cells than in any other fetal or adult cells [12]. Gene knockout mice lacking expression of B-Myb die at E4.5–6 [13], highlighting the importance of the protein during the early stages of embryonic development and suggesting that it might have a role in ESCs. However, the role of B-Myb in ESCs remains unclear even though attempts to address this issue using *B-myb* shRNA knockdown have suggested that the early lethality (E4.5–6.5) in the *B-myb* knockout is due to deregulated expression of the pluripotency-associated proteins, Oct-4 (MGI:101893) and Sox-2 (MGI:98364) [12].

To gain an insight into the role of B-Myb in ESCs, we have generated genetically modified cells in which we can control *B-myb* gene deletion. We have found that B-Myb ablation does not affect the expression of pluripotency factors in ESCs, but rather it has profound effects on S phase that could also explain the genome instability observed when the levels of the protein are reduced. Our results shed light on the mechanisms involved in the high proliferative capacity of ESCs and the maintenance of genomic integrity. The understanding of these basic processes is essential for the effective translational application of ESCs.

Materials and Methods

Generation of Embryonic Stem Cells

ESCs were generated by standard protocols [14] from crosses between $B\text{-}myb^{+/\Delta}$ and $B\text{-}myb^{F/F}$ mice [15].

Europe PMC Funders Author Manuscripts

Cell Culture and Conditional Gene Deletion

TL1, CJ7, *c-myc*$^{-/-}$, *B-myb*$^{+/\Delta}$, *B-myb*$^{F/\Delta}$, and *B-myb*$^{\Delta/\Delta}$ ESCs were cultured and expanded under standard ESCs culture conditions. To induce *B-myb* deletion in *B-myb*$^{+/\Delta}$ and *B-myb*$^{F/\Delta}$ ESCs, cells were transfected with pLv-Cre-eGFP plasmid [16] (10 μg) using the Amaxa nucleofection technology (Amaxa, Köln, Germany, www.lonzabio.com). Green Fluorescent Protein-positive (GFP) cells were sorted 48 hours after transfection using a Cytomation MoFlo machine, and they were used immediately or placed back into culture over feeders for another 48 hours.

B-myb$^{F/\Delta}$ ESCs transfected with pLv-Cre-eGFP plasmid were sorted 48 hours after transfection and placed back into culture over feeders. Eight individual clones were isolated and checked for absence of expression of B-Myb. Two of the clones were used for performing rescue experiments.

Immunohistochemistry

Blastocysts were placed onto gelatinized culture slide chambers (Falcon, Becton Dickinson, Franklin Lakes, NJ, www.bdbiosciences.com) containing ESCs medium and outgrowths fixed after 72 hours. ESCs were cultured on irradiated Mouse Embryonic Fibroblasts (MEF) on glass coverslips. Immunostaining was performed according to standard protocols. Samples were incubated overnight with primary antibodies, anti-Oct-4 (1:200 monoclonal antibody, Santa Cruz Biotechnology, Santa Cruz, CA, www.scbt.com) and anti-TROMA-1 (anti-cytokeratin 8) monoclonal antibody (1:20; Developmental Studies Hybridoma Bank (DSHB), Iowa City, IA, http://dshb.biology.uiowa.edu/), followed by incubation with appropriate AlexaFluor-conjugated secondary antibodies, and mounted using DAPI-containing Vectashield (Vector Laboratories, Peterborough, UK, www.vectorlabs.com). Samples were analyzed using confocal fluorescence microscopy. Outgrowths were processed individually for B-*myb* genotype determination by polymerase chain reaction (PCR) using primers as previously described [15]. Blastocyst out-growths homozygous for the wild-type or deleted alleles are designated *B-myb*$^{+/+}$ and *B-myb*^{null}, respectively.

Proliferation Assay

A total of 10^5 GFP-positive sorted cells of *B-myb*$^{+/\Delta}$ and *B-myb*$^{\Delta/\Delta}$ ESCs were seeded over irradiated MEFs on a 6-cm plate. Growth medium was replaced every 24 hours. Cells were harvested and counted in triplicate after 48 and 96 hours using the Trypan blue exclusion method.

Western Blotting

Fifty micrograms of total protein extract was used for western blot as previously described [9]. Antibodies were as follows: anti-B-Myb mouse monoclonal (1:1,000 dilution, Santa Cruz Biotechnology, Santa Cruz, CA, www.scbt.com), anti-Oct-4 mouse monoclonal (1:1,000 dilution, Santa Cruz Biotechnology, Santa Cruz, CA, www.scbt.com), anti-rabbit Histone Deacetylase 1 (HDAC1) polyclonal (1:1,000 dilution, a generous gift from by Dr Laura O'Neill, University of Birmingham), and anti-Sox-2 mouse monoclonal (1:500 dilution, R&D systems, Minneapolis, MN, www.rndsystems.com).

Analysis of H2AXγ by Flow Cytometry

Ninety-six hours after transfection with Cre recombinase, *B-myb*$^{+/\Delta}$ and *B-myb*$^{\Delta/\Delta}$ ESCs were collected and fixed in 4% paraformaldehyde / 2% sucrose for 10 minutes. After permeabilization (20 mM HEPES pH 7.4, 50 mM NaCl, 3 mM $MgCl_2$, 300 mM sucrose 0.5% TritonX-100) for 5 minutes at 4 °C, cells were incubated for 30 minutes with anti-phospho-Histone H2A.X (Ser139; 1:100 diluted mouse monoclonal clone JBW301, Millipore) followed by goat anti-mouse-AlexaFluor 488 (A11029, Invitrogen). Labeled cells were washed and resuspended in propidium iodide (5 μg/ml) in phosphate buffer saline (PBS), then processed with a Cyan flow cytometer (Beckman Coulter, Brea, CA, www.beckmancoulter.com). Acquired data was analyzed using Summit (Dako, Beckman Coulter; Fig. 3e) or FlowJo (Tree Star Inc; Supporting Information Figure S3b) software. Experiments were performed in triplicate.

Immunofluorescence Staining of Replication Foci Using Bromodeoxyuridine or Iododeoxyuridine

ESCs were cultured on MEFs on glass coverslips in the presence of 25 μM bromodeoxyuridine (BrdU; Sigma-Aldrich, St Louis, MO, www.sigmaaldrich.com) for 20 minutes followed (or not) by 250 μM iododeoxyuridine (IdU; Sigma-Aldrich, St Louis, MO, www.sigmaaldrich.com) for 25 minutes. The cells were then fixed in ethanol/acetic acid (95%:5%) for 20 minutes and incubated with 1 N HCl for 30 minutes. After several washes in distilled water and RNase treatment (100 μg/ml, 30 minutes at 37 °C), cells were incubated overnight with monoclonal rat anti-BrdU antibody (1:100 dilution, clone BU1/75, Abcam, Cambridge, UK, www.abcam.com ab6326) followed by donkey anti-rat-AlexaFluor 488 (1:1,000 dilution, Invitrogen, Paisley, UK, www.invitrogen.com A21208). When double labeling was performed, this was followed by an overnight incubation with monoclonal mouse anti-IdU antibody (1:100 dilution, Invitrogen, Paisley, UK, www.invitrogen.com MD5000), then with goat anti-mouse AlexaFluor 594 antibody (1:1000 dilution, Invitrogen, Paisley, UK, www.invitrogen.com A11032). Cells were mounted using DAPI-containing Vectashield (Vector Laboratories, Peterborough, UK, www.vectorlabs.com). A minimum of two coverslips were analyzed per sample per experiment and experiments were performed in triplicate. Images were acquired by confocal fluorescence microscopy (×100 oil immersion objective) and analyzed for their S phase pattern [17] and the architecture of their replication factories. A minimum of 100 cells per sample was scored, and a minimum of 15 nuclei was analyzed per sample, z-stack of 0.4-μm sections being made for each nucleus.

DNA Fiber Analysis

Replication tracks were labeled in culture medium containing 25 μM BrdU (Sigma-Aldrich, St Louis, MO, www.sigmaaldrich.com). For dual labeling, cultures were pulse-labeled with 25 μM BrdU, washed, and then labeled with 250 μM IdU (Sigma-Aldrich, St Louis, MO, www.sigmaaldrich.com). DNA fiber spreads were prepared as previously described [18]. BrdU-labeled tracks were detected with rat anti-BrdU antibody (1:1,000 dilution, Abcam, Cambridge, UK, www.abcam.com ab6326) overnight at 4 °C (or 1 hour at room temperature in case of dual labeling) using donkey anti-rat-AlexaFluor 488 (1:500 dilution, Invitrogen, Paisley, UK, www.invitrogen.com A21208). IdU-labeled tracks were detected with sheep

anti-BrdU (1:500 dilution, Biodesign M20105S) overnight at 4 °C and donkey anti-sheep-AlexaFluor 594 (Invitrogen, Paisley, UK, www.invitrogen.com, A11016). To eliminate any broken or tangled DNA fibers, DNA was systematically labeled with monoclonal mouse anti-human ssDNA antibody using AlexaFluor 594- or AlexaFluor 405-conjugated goat anti-mouse secondary antibodies (1:500 dilution, Invitrogen, Paisley, UK, www.invitrogen.com, A11032 or A31553) for single or dual labeling, respectively. Slides were mounted in ProLong Gold antifade reagent. A minimum of three slides were analyzed per sample per experiment, and a minimum of 140 forks per sample was counted. Images were acquired by confocal fluorescence microscopy, and labeled tracks were measured with the Zeiss LSM Image Browser v4.2 using a conversion factor of 1 μm = 2.59 kbp [18]. The frequency of origins was calculated as described [19].

Quantitative Reverse Transcriptase-PCR (qRT-PCR)

Real time PCR was carried out using either SYBRGreen or TaqMan PCR master mix depending on the primers. One microliter of cDNA dilution was used in a 20 μl reaction. The reaction was carried out in a Stratagene Mx3000P machine. At least two separate reactions with three replicates per sample were run. Relative gene expression was calculated as $2^{-\Delta\Delta Ct}$ values with β2 microglobulin as a control. Taqman primers and probes were as follows:

B-myb F: 5′-GGGCTGAGATCGCCAAGAT-3′

B-myb R: 5′-CCGTGTCGACTTTCCTTTTGA-3′

B-myb Probe: 5′-FAM-CAGGGAGGACGGACAATGCTGTGAA-BHQ1-3′

β2 Microglobulin F: 5′-CATACGCCTGCAGAGTTAAGCA-3′

β2 Microglobulin R: ATCACATGTCTCGATCCCAGTAGA-3′

β2 Microglobulin Probe: 5′-VIC-CAGTATGGCCGAGCCCAAGACCG-BHQ1-3′

Cenpf F: GAAGACGAAAGTGGAATTGATTGAA-3′

Cenpf R: 5′-CGGTGACAACTCAACTCCTCAG-3′

Cenpf Probe 5′-FAM- ACAGTATGACCAGGCCGCAGCCAA-BHQ1-3′

c-myc (Mm00487803-m1, Applied Biosystems)

Cdc2a, Cenpe, and *Ccna2* sequences were as described [20]. SYBRGreen primers sequences for *FoxM1, Cdc25b, AurkB*, *Survivin*, and *Ccnb1* were as described [21].

Microscopy

All images were acquired using a Zeiss LSM 510 Meta confocal microscope with the exception that images of alkaline phosphatase staining were obtained with an inverted microscope Olympus CKX41 equipped with a digital camera. Zeiss LSM Image Browser

v4.2 was used for basic analysis of the confocal images (Carl Zeiss Ltd., Hertfordshire, UK, www.zeiss.co.uk).

Imaris Three-Dimensional Visualization and Quantitation

Z-stacks of confocal images of nuclei were uploaded into Imaris x64.3.1 (Bitplane, Zurich, Switzerland, www.bitplane.com). The colocalization function of Imaris was used to detect colocalized pixels. The Region of Interest was defined as above a threshold of three on the red channel. The automatic threshold was used on 10 nuclei of *B-myb*$^{+/\Delta}$ ESCs, and average thresholds were defined for green and red channels and used to analyze all *B-myb*$^{+/\Delta}$ and *B-myb*$^{\Delta/\Delta}$ ESC nuclei. The colocalized pixels were colored white and used to generate a colocalization channel and Pearson's correlation coefficient (r) in the colocalized volume. The coefficient of determination (r^2) was then calculated.

The green (BrdU) and red (IdU) channels were used to generate the three-dimensional (3D) spots corresponding to replication factories. The spots function in Surpass in Imaris was used. Spots were defined as "growing regions" of an estimated diameter of 0.3 μm. Other filters were kept in automatic mode except Spot regions, defined manually at diameter 5 from the region border. The software assigns an identification number to each of the spots generated, and gives for each spot its signal intensities for each channel and its diameter. These data were used to assess if the size and signal intensities of the replication factories were affected between *B-myb*$^{+/\Delta}$ and *B-myb*$^{\Delta/\Delta}$ ESCs. In addition, the software quantifies the number of spots for each channel and this was used to estimate the number of replication foci.

Cross-linking Chromatin Immunoprecipitation (X-ChIP)

X-ChIP was performed as described in the manufacturer's protocol (Abcam). The elution step was changed for the Q2 method [22]. The chromatin of CJ7 and TL1 ESCs lines was incubated overnight with 8 μg of rabbit IgG or B-Myb antibody (Santa Cruz Biotechnology, Santa Cruz, CA, www.scbt.com) preconjugated to proteins A and G agarose/ssDNA. Equal amount of DNA was used for real time PCR analysis with appropriate primer pairs for B-Myb-binding sites in the *c-myc* and *FoxM1* genes (Supporting Information Table S1).

Rescue Experiments

The mouse *FoxM1* cDNA and the mouse *c-myc* cDNA were inserted into a vector containing an Internal Ribosome Entry Site (IRES) element and a red fluorescent protein (DsRed), the pIRES2 DsRed-Express2 vector (Clontech, St-Germain-en-Laye, France, www.clontech.com), using the restriction enzymes BamHI and XhoI respectively. These plasmids were named as FoxM1/dsRED and *c-Myc*/dsRED.

Two *B-myb*$^{\Delta/\Delta}$ ESC clones were transfected with pIRES2 DsRed-Express2 as control plasmid (control/dsRED), FoxM1/dsRED or c-*myc*/dsRED plasmids, as explained earlier. Red-positive cells were sorted 48 hours after transfection using a Cytomation MoFlo machine, and placed back into culture over feeders for another 24 hours. Cells were processed for DNA fiber analysis as described earlier.

Statistical Analysis

Statistical analyses were performed using SPSS v15 (SPSS Inc.) and Prism4 v4.03 (GraphPad Software). When comparing data sets between *B-myb*$^{+/\Delta}$ and *B-myb*$^{\Delta/\Delta}$ ESCs, two-tailed unpaired Student's *t*-test was used and the unequal variance correction was applied when indicated. When comparing data with small sample sizes, a two-tailed Mann-Whitney test was performed because the Gaussian distribution of the population could not be assumed. However, for Figure 3E, unpaired Student t-test was used to analyze the experiment which has a small sample size only because the statistical power (post-hoc) was high enough (80%). For nominal variables (the different types of replication structures or the different S phase patterns observed) a two-tailed v^2 contingency test was used. For all tests, a *p* value lower than .05 was considered significant.

Results and Discussion

B-Myb Ablation Does Not Affect Expression of the Pluripotency-Associated Proteins Oct-4 and Sox-2

To elucidate the in vivo function of B-Myb, we have generated *B-myb*$^{+/\Delta}$ and *B-myb*$^{F/\Delta}$ ESCs in which the F allele can be deleted on activation of Cre recombinase [15], generating *B-myb*$^{\Delta/\Delta}$ cells that lack any expression of the transcription factor. The pluripotency of the ESC lines generated was assessed by: (a) staining for the stem cell membrane marker alkaline phosphatase, (b) immunostaining for the pluripotency marker Oct-4, and (c) their capacity to generate chimeras (Fig. 1A-1C). To completely delete *B-myb* gene function, *B-myb*$^{F/\Delta}$ ESCs were transfected with a Cre-eGFP expressing plasmid followed by sorting of GFP^{+} cells. *B-myb*$^{+/\Delta}$ ESC transfected with Cre-eGFP were used as the control as, like *B-myb*$^{F/\Delta}$ ESCs, they express half the normal levels of B-Myb prior to transfection. The successful ablation of B-Myb was assessed by western blot. A saturated exposure of the membrane showed only trace levels of B-Myb protein (Fig. 1D), which is most likely due to contamination with GFP-negative cells following sorting. Under these conditions, we found that the levels of Oct-4 and Sox-2 proteins were unaffected by the loss of B-Myb (Fig. 1D). Furthermore, immunostaining of *B-myb*$^{+/+}$ and *B-myb*^{null} blastocyst outgrowths revealed similar levels of Oct-4 expression (Fig. 1E). A previous publication claimed coordinated changes in B-Myb and Oct-4 expression [12]. Our data, however, demonstrate that B-*myb*^{null} blastocysts and ESCs in which *B-myb* has been conditionally deleted both express Oct-4 and Sox-2, thus ruling out the possibility of B-Myb acting as a master regulator of the critical regulators of pluripotency. This difference with the earlier publication may be the consequence of their shRNA approach, which might be inefficient in reducing the very high expression levels of B-Myb in ESCs, thus making the experimental conditions suboptimal and the results difficult to interpret. We consider that our conditional gene-targeting approach is more appropriate when dealing with high-abundance proteins such as B-Myb, as the process is irreversible and de novo transcription of the gene to compensate for induced low levels cannot occur.

On the basis of these findings, we hypothesized that the failure of ICM progression in *B-myb* knockout embryos is due to impaired proliferation leading to genome instability, rather

than to a role of B-Myb as a modulator of the expression of pluripotency-associated proteins.

B-Myb Ablation Results in a Superactivation of Replication Factories

Next, we compared the proliferation capacity of *B-myb*$^{+/\Delta}$ and *B-myb*$^{\Delta/\Delta}$ ESCs for a period of 4 days following gene deletion by Cre recombinase. *B-myb*$^{\Delta/\Delta}$ ESCs showed a remarkable reduction in their proliferative capacity when compared with *B-myb*$^{+/\Delta}$ cells (Supporting Information Figure S1A). Cells lacking B-Myb were negative for TUNEL staining, thus ruling out the possibility of an apoptotic effect (data not shown). Progression through S phase can be determined in whole cells by BrdU incorporation and subsequent immunofluorescence analysis, allowing for subdivision into early, mid, and late stages based on the specific patterns of replication foci pattern [17]. After *B-myb* deletion in *B-myb*$^{F/\Delta}$ ESCs, analysis of the pattern of replication foci following BrdU incorporation revealed a reduction in the percentage of cells in early S phase and a twofold increase in the percentage of cells in late S phase (Supporting Information Figure S1B). This data suggests that the absence of B-Myb might affect the duplication time of the genome and the overall S phase program, prompting us to examine the global architecture of the replication machinery using incorporation of halogenated deoxynucleosides. First, using high-resolution 3D imaging in single cells, we observed that ablation of B-Myb affects the number of replication foci in early S phase, with the majority of *B-myb*$^{+/\Delta}$ ESCs (94%) having less than 500 foci/cell compared with only 65% of the *B-myb*$^{\Delta/\Delta}$ cells, although 35% of these had more than 1,000 foci/cell (Fig. 2A, 2B and Supporting Information Fig. S2A). Nevertheless, using consecutive pulses of halogenated deoxynucleosides (BrdU and IdU) in early S phase, we found no differences in the percentage of colocalization (Fig. 2C, 2D), indicating that the active replication foci stayed spatially coupled. Moreover, there was no significant difference in the size or intensity of replication foci (Supporting Information Fig. S2B-C). Taken together, these findings demonstrate a superactivation of replication factories in *B-myb*$^{\Delta/\Delta}$ ESCs, without an effect on the spatial sequential activation of the replicons.

B-Myb Ablation Affects Replication at the Level of Single DNA Fibers

We extended our analysis to investigate replication dynamics at the level of single DNA fibers. *B-myb*$^{+/\Delta}$ and *B-myb*$^{\Delta/\Delta}$ ESCs were subjected to a short pulse of BrdU, and spread DNA fibers from these cells were used to analyze single active replicons by measuring the average length of BrdU-labeled replication forks, as well as their elongation rate. Confocal images obtained from *B-myb*$^{\Delta/\Delta}$ cells were noticeably different, with the BrdU-labeled tracks being much shorter than in the controls (Fig. 3A and Supporting Information Fig. S3A). *B-myb*$^{\Delta/\Delta}$ ESCs displayed a striking reduction in the length of active replication forks relative to the controls, with a majority (76%) of the forks ranging from 5 to 20 kbp, while 69% of *B-myb*$^{+/\Delta}$ extended from 30 to 55 kbp. On average, the rate of fork elongation was reduced by approximately twofold in the absence of B-Myb (0.7 ± 0.48 compared with 1.7 ± 0.73 kbp/minute; Fig. 3A, 3B). Moreover, we determined the different proportions of replication structures using consecutive pulses of two different halogenated deoxynucleosides, BrdU and IdU (Fig. 3C, 3D). Loss of B-Myb profoundly affected the proportion of replicon structures; in fact, a direct comparison between *B-myb*$^{+/\Delta}$ and *B-myb*$^{\Delta/\Delta}$ ESCs revealed that the percentage of consecutive labeling forks (ongoing forks) was

considerably reduced (from 74.4% in the controls to 38.3%), but that there was increase in the percentage of termination (from 13.1% to 21%), stalling (from 1.3% to 21%) and interspersed (from 0.6% to 3.3%) forks. In addition, there was an increase in the frequency of new activated origins of replication from 14% in *B-myb*$^{+/\Delta}$ to 39% in *B-myb*$^{\Delta/\Delta}$ ESCs, which is probably the result of a balancing mechanism to compensate for the low rate of elongation at replication forks by increasing the number of origins being fired [23].

The aforementioned results demonstrate that the lack of B-Myb induces fork stalling, which can be a source of genome instability as stalled forks that are not resolved can collapse and give rise to unreplicated chromosomal regions [24]. Double-strand breaks (DSB) serve as docking sites for the accumulation of H2AXγ (histone H2AX phosphorylated on serine 139) at the lesion, making this an invaluable marker for measuring DNA damage [25]. Hence, we quantified the presence of DSB by measuring the accumulation of the histone H2AXγ using flow cytometry. A 40% increase in the levels of H2AXγ was observed in *B-myb*$^{\Delta/\Delta}$ ESCs relative to *B-myb*$^{+/\Delta}$ ESCs (Fig. 3E and Supporting Information Fig. S3B). Surprisingly, this increase in H2AXγ was not specific to cells in S phase, as demonstrated by costaining with propidium iodide, suggesting that the S phase and G2/M checkpoint controls are compromised in the absence of B-Myb, allowing cells carrying genetic modifications to progress through the cell cycle. The reduction in the fork length and the increase of DSB are similar to that seen in response to DNA damage or replication stress occurring during normal S phase or after exposure to DNA-damaging factors. The same phenotype has been observed following inhibition of the Chk-1/ATR pathway [23], when topoisomerase activity is compromised [24] or when DNA precursor pools are reduced [26]. In all of these situations, the intra S phase checkpoint acts as a sensor that triggers a molecular response aimed at delaying cell cycle progression and entrance into mitosis, thereby allowing time for repair of DNA lesions; a failure to do so would result in mutations, genome instability, or cell death [27].

B-Myb Regulates *c-myc* and *FoxM1* Expression

Our data reveal a defect in the dynamics of replication in ESCs in the absence of B-Myb. To identify potential causative B-Myb targets, we quantified the expression of selected genes known to be involved in S phase progression or G2/M transition, in particular focusing on those previously shown to be regulated by B-Myb in other cell types [20, 28, 29]. RNAs encoding two multifunctional proteins implicated in cell cycle regulation, namely c-Myc (MGI:97250) and FoxM1 (MGI:1347487), were dramatically downregulated in *B-myb*$^{F/\Delta}$ ESCs 48 hours after transfection with Cre recombinase (Fig. 4A). This result fits with the replication phenotype observed in *B-myb*$^{\Delta/\Delta}$ ESCs. Hence, c-Myc has a direct role in the control of DNA replication, interacts with the prereplicative complex and localizes to early sites of DNA synthesis [30], while FoxM1 is a proliferation-associated transcription factor regulating S phase progression [31]. Moreover, a novel function for FoxM1 has recently been reported with respect to the transcriptional response during DNA damage/checkpoint signaling, whereby cells treated with siRNA for *FoxM1* displayed an increase in DNA breaks [32]. The association between low levels of FoxM1 and an increase in DSB is consistent with our results as we observed an increase in the number of DSB measured by H2AXγ staining when B-Myb is ablated.

Both c-Myc and FoxM1 are known to regulate a plethora of cell cycle-associated genes and, because of their functional relevance, we chose to assess the effect of B-Myb ablation on the expression of the FoxM1-regulated genes *AurkB* (MGI:107168), *Cenpf* (MGI:1313302), *Cenpe* (MGI:1098230), *Survivin* (also known as *Birc5*) (MGI:1203517), *Ccnb1* (MGI: 88302), and *Cdc25b* (MGI:99701), and of the c-Myc-regulated genes *Plk1* (MGI:97621), *Cdc2a* (also known as *Cdk1*) (MGI:88351), and *Ccna2* (MGI:108069) (Fig. 4A). Interestingly, these genes exhibited distinct responses on ablation of B-Myb (Fig. 4A); the genes for the S phase-associated proteins Cdc25b, necessary for the activation of cyclin-cdk [33, 34] and Plk1, which interacts with prereplicative complex proteins such as Mcm2 (MGI:105380) and Orc2 (MGI:1328306) [35, 36], being rapidly downregulated, whereas the expression of *Ccnb1, Ccna2*, *Cdc2a*, *Cenpf, AurkB*, and *Survivin*, which encode proteins involved in the G2/M transition and M phase progression, were not altered 48 hours after transfection of *B-myb*$^{F/\Delta}$ cells with Cre recombinase, although a decline in expression was detectable at 11 days (Supporting Information Fig. S4). These findings indicate that genes encoding proteins involved in the prereplicative complex and S phase progression are likely primary targets of B-Myb, whereas genes previously implicated as direct B-Myb targets that encode for proteins related to the G2/M transition, appear in this system to be affected as an indirect consequence of B-Myb ablation.

Next, we investigated whether the decreased expression of *c-myc* and *FoxM1* was the result of direct gene-transcriptional regulation following deletion of B-Myb. The activation of the *c-myc* gene by B-Myb has been a subject of study for many years, although results so far have been inconclusive. This may in part be the consequence of the experimental approaches utilized so far, which have been based on transient cotransfection/reporter assays that render no information regarding the true in vivo transcriptional regulation of endogenous genes. For instance, transcriptional activation of the human c-*myc* gene by both human c-Myb and B-Myb were shown to activate the human c-*myc* gene [37], whereas using the same experimental approach, the murine c-*myc* promoter was transactivated by murine c-Myb but not murine B-Myb [38].

We looked for direct links between B-Myb and gene regulation using chromatin immunoprecipitation (ChIP) with an anti-B-Myb antibody, enabling detection of in vivo binding of B-Myb to potentially functional Myb recognition elements (MREs). We identified three putative MREs in the *FoxM1* gene at −3.5, −2.7 and −2.1 kbp from the ATG (Supporting Information Fig. S5A). We also identified 10 putative B-Myb binding sites within a region of two kbp surrounding the first exon of *c-myc*. Four of these sites, located at approximately −1.7, −1.2, −0.78, and +.028 kbp relative to the ATG, showed some degree of conservation as judged by multispecies alignments of the syngenic genomic regions (Supporting Information Fig. S5B). We performed ChIP on cross-linked chromatin from two different ESC lines, enrichment of specific DNA segments containing the aforementioned consensus B-Myb binding sequences within the *FoxM1* and *c-myc* genes being assessed by quantitative PCR using specific primers. Specific enrichment indicative of in vivo binding of B-Myb was observed at the *FoxM1* locus in the binding site 2 region (BS2), which also displays the highest sequence conservation between species (Supporting Information Fig. S5A). The level of enrichment was consistently reproducible among chromatin preparations (Fig. 4B, upper panel). Even though putative B-Myb binding sites in the *FoxM1* promoter

have been suggested from comparative genomics analysis [39], this is the first demonstration of in vivo binding of B-Myb to a specific site within the *FoxM1* gene, confirming that *FoxM1* is a direct target gene for regulation by B-Myb. Specific enrichment was also observed at the BS3 region of the *c-myc* gene (located at 0.78 kbp), although this level of enrichment was more variable compared with that seen on *FoxM1* (Fig. 4B, lower panel), which could be due to weaker binding of B-Myb to the *c-myc* promoter or perhaps to technical limitations, such as the B-Myb epitope being partially masked when the transcription factor is bound to DNA in the context of the *c-myc* promoter.

c-myc Null ESCs Exhibit Defects on DNA Replication at the Level of Single DNA Fiber

Deletion of the *B-myb* gene leads to a replication phenotype characterized by a drastic reduction in replication fork velocity. Our combined real-time PCR and X-ChIP data suggest that this effect could be the result of B-Myb regulating important cell cycle genes such as *c-myc* and *FoxM1*. We reasoned that if a reduction in *c-myc* and *FoxM1* expression was responsible for the observed phenotype, $c\text{-}myc^{-/-}$ and $FoxM1^{-/-}$ ESCs should also display such impairment on replication-fork elongation.

Constitutive and conditional knockout *FoxM1* mouse lines have both been described [40, 41] but no $FoxM1^{-/-}$ ESCs are presently available, preventing us from an equivalent investigation of the effect of FoxM1 on replication fork elongation in ESCs. However, we were able to obtain $c\text{-}myc^{-/-}$ ESCs [42], which we used to perform the same type of replication studies as those described for $B\text{-}myb^{+/\Delta}$ and $B\text{-}myb^{\Delta/\Delta}$ ESCs. $c\text{-}myc^{-/-}$ ESCs, which grow with a reduced duplication time (data not shown), were subjected to a short pulse of BrdU, and spread DNA fibers were analyzed for single active replicons by measuring the average length of BrdU-labeled replication forks, as well as their elongation rate. As expected, $c\text{-}myc^{-/-}$ ESCs displayed considerably shorter active replication forks relative to those observed in $B\text{-}myb^{+/\Delta}$, with a majority of the forks (76%) ranging from 15 to 35 kbp. On average, the rate of fork elongation was 1.0 ± 0.47 kbp/minute (Fig. 5A). This data is in agreement with our hypothesis that the DNA replication phenotype observed in the absence of B-Myb can be the consequence of c-Myc downregulation. The reduction in replication fork progression in $B\text{-}myb^{\Delta/\Delta}$ ESCs is greater than that observed for $c\text{-}myc^{-/-}$ ESCs, indicating that *c-myc* is probably not the only B-Myb target gene product responsible for the $B\text{-}myb^{\Delta/\Delta}$ ESCs replication phenotype.

Overexpression of c-myc and FoxM1 Rescues the $B\text{-}Myb^{\Delta/\Delta}$ ESC Replication Phenotype

The aforementioned results persuaded us to attempt to rescue the $B\text{-}myb^{\Delta/\Delta}$ ESCs replication phenotype by ectopic expression of c-Myc and FoxM1. c-*myc* and *FoxM1* cDNAs were subcloned into the pIRESdsRedExpress2 vector (referred to as c-*myc*/dsRED and FoxM1/dsRED, respectively), and in each set of experiments, $B\text{-}myb^{\Delta/\Delta}$ ESCs were transfected either with c-*myc*/dsRED, FoxM1/dsRED, or empty vector (control/dsRED). Transfected cells were sorted on the basis of red fluorescent protein expression and subjected to a short pulse of BrdU. Spread DNA fibers from the labeled cells were used to analyze single active replicons by measuring the average length of BrdU-labeled replication forks, as well as their elongation rate. $B\text{-}myb^{\Delta/\Delta}$ ESCs transfected with control/dsRED exhibited similar replication kinetics to $B\text{-}myb^{\Delta/\Delta}$ ESCs, with a majority of the forks (78%) ranging from 10

to 25 kbp, and an average fork elongation rate of 0.7 ± 0.45 kbp/minute (Fig. 5B). *B-myb*$^{\Delta/\Delta}$ ESCs transfected with FoxM1/dsRED, on the other hand, showed a mild recovery, with an average fork elongation rate of 1.0 ± 0.64 kbp/minute (1.4-fold increase compared with vector alone). Overall, the expression of FoxM1 gave rise to a modest increase on the average active replication fork length (25.2 ± 15 kbp compared with 18.7 ± 11.2 kbp), with 86% of the forks ranging from 10 to 40 kbp (Fig. 3B, lower panel). In contrast, *B-myb*$^{\Delta/\Delta}$ ESC transfected with the c-*myc*/dsRED plasmid exhibited an increase in the rate of fork elongation by approximately twofold compared with the *B-myb*$^{\Delta/\Delta}$ ESC control (1.5 ± 0.76 compared with 0.7 ± 0.45 kbp/minute), with the majority of the forks (66%) ranging from 20 to 50 kbp, with an average active replication fork length of 37.6 ± 19.1 kbp (Fig. 5B, upper panel). Altogether, these data show a partial rescue of the *B-myb*$^{\Delta/\Delta}$ replication phenotype. Although fork velocity is not completely recovered by c-Myc, an average fork elongation rate of 1.5 kbp/minute is considered normal in mammalian cells [18, 43].

Overall, we present compelling evidence showing that the replication phenotype observed in ESC on deletion of *B-myb* is due to aberrant transcriptional regulation of the cell cycle proliferation factors, c-Myc and FoxM1. This adds to previous reports showing that c-Myc can bind to the promoters of *FoxM1* and *B-myb*, and also that the *c-myc* gene is a direct target of FoxM1, suggesting that a crossregulation between c-Myc and FoxM1 takes place during cell replication events [31, 44]. Our results broaden these observations by introducing B-Myb into the picture, whereby direct transcriptional regulation of FoxM1 by B-Myb, and a feedback loop between the latter and c-Myc, may be governing the replication machinery in ESCs, as depicted in the model proposed in Figure 6.

Summary

We have demonstrated that the loss of B-Myb in ESCs in the absence of DNA damage or replication stress has multiple consequences that profoundly impact the ability of the cells to proliferate and maintain their genome stability, including (a) a significant slowdown in their proliferation rate, (b) disturbance of S phase progression, (c) a superactivation of active replication foci, (d) an effect on the elongation rate of replication forks, and (e) impaired maintenance of replication fork stability leading to an increase in DSB. We propose that the effect of B-Myb deletion on genome stability is a consequence of two consecutive events, that is, improper S phase progression followed by a failure of the G2/M-phase progression, ultimately affecting genome integrity [9, 12, 20]. Moreover, B-Myb seems to act as a key component of the cellular machinery that dictates normal S phase progression through the regulation of *c-myc* and *FoxM1*, thus placing B-Myb at the heart of cell cycle gene regulation in ESCs.

Supplementary Material

Refer to Web version on PubMed Central for supplementary material.

Acknowledgments

We thank Andrea Bacon for help with the generation of chimeras. We are also grateful to Oscar Berlanga for critical reading of the manuscript. The hybridoma TROMA-I developed by Philippe Brulet and Rolf Kemler was

obtained from the Developmental Studies Hybridoma Bank developed under the auspices of the NICHD and maintained by The University of Iowa, Department of Biological Sciences (Iowa City, IA). We are very grateful to Allan Bradley for providing the *c-myc*$^{-/-}$ ESCs, to Rene Medema for the mouse cDNA of *FoxM1*, to Edward V. Prochownik for the mouse *c-myc* cDNA, and to Joost Verhaagen for the LV-Cre-eGFP plasmid. This work was supported by the Grant BB/E001459/1 from the Biotechnology and Biological Sciences Research Council (BBSRC, U.K.).

References

1. Niwa H. How is pluripotency determined and maintained? Development. 2007; 134:635–646. [PubMed: 17215298]
2. Kim JM, Nakao K, Nakamura K, et al. Inactivation of Cdc7 kinase in mouse ES cells results in S-phase arrest and p53-dependent cell death. EMBO J. 2002; 21:2168–2179. [PubMed: 11980714]
3. Rossi DJ, Londesborough A, Korsisaari N, et al. Inability to enter S phase and defective RNA polymerase II CTD phosphorylation in mice lacking Mat1. EMBO J. 2001; 20:2844–2856. [PubMed: 11387217]
4. Yoshida K, Kuo F, George EL, et al. Requirement of CDC45 for postimplantation mouse development. Mol Cell Biol. 2001; 21:4598–4603. [PubMed: 11416137]
5. Brown EJ, Baltimore D. ATR disruption leads to chromosomal fragmentation and early embryonic lethality. Genes Dev. 2000; 14:397–402. [PubMed: 10691732]
6. Takai H, Tominaga K, Motoyama N, et al. Aberrant cell cycle checkpoint function and early embryonic death in Chk1(−/−) mice. Genes Dev. 2000; 14:1439–1447. [PubMed: 10859163]
7. Sala A. B-MYB, a transcription factor implicated in regulating cell cycle, apoptosis and cancer. Eur J Cancer. 2005; 41:2479–2484. [PubMed: 16198555]
8. Fung SM, Ramsay G, Katzen AL. Mutations in Drosophila myb lead to centrosome amplification and genomic instability. Development. 2002; 129:347–359. [PubMed: 11807028]
9. Garcia P, Frampton J. The transcription factor B-Myb is essential for S-phase progression and genomic stability in diploid and polyploid megakaryocytes. J Cell Sci. 2006; 119:1483–1493. [PubMed: 16551698]
10. Manak JR, Mitiku N, Lipsick JS. Mutation of the Drosophila homologue of the Myb protooncogene causes genomic instability. Proc Natl Acad Sci USA. 2002; 99:7438–7443. [PubMed: 12032301]
11. Shepard JL, Amatruda JF, Stern HM, et al. A zebrafish bmyb mutation causes genome instability and increased cancer susceptibility. Proc Natl Acad Sci USA. 2005; 102:13194–13199. [PubMed: 16150706]
12. Tarasov KV, Tarasova YS, Tam WL, et al. B-MYB is essential for normal cell cycle progression and chromosomal stability of embryonic stem cells. Plos One. 2008; 3:e2478. [PubMed: 18575582]
13. Tanaka Y, Patestos NP, Maekawa T, et al. B-myb is required for inner cell mass formation at an early stage of development. J Biol Chem. 1999; 274:28067–28070. [PubMed: 10497154]
14. Hogan, B.; Beddington, R.; Costantini, F., et al. Manipulating the Mouse Embryo. Cold spring Harbor Laboratory Press; New York: 1994. p. 497
15. Garcia P, Berlanga O, Watson R, et al. Generation of a conditional allele of the B-myb gene. Genesis. 2005; 43:189–195. [PubMed: 16283626]
16. Ahmed BY, Chakravarthy S, Eggers R, et al. Efficient delivery of Cre-recombinase to neurons in vivo and stable transduction of neurons using adeno-associated and lentiviral vectors. BMC Neuroscience. 2004; 5:4. [PubMed: 15005815]
17. Ferreira J, Paolella G, Ramos C, et al. Spatial organization of large-scale chromatin domains in the nucleus: A magnified view of single chromosome territories. J Cell Biol. 1997; 139:1597–1610. [PubMed: 9412456]
18. Jackson DA, Pombo A. Replicon clusters are stable units of chromosome structure: Evidence that nuclear organization contributes to the efficient activation and propagation of S phase in human cells. J Cell Biol. 1998; 140:1285–1295. [PubMed: 9508763]

19. Conti C, Seiler JA, Pommier Y. The mammalian DNA replication elongation checkpoint: Implication of Chk1 and relationship with origin firing as determined by single DNA molecule and single cell analyses. Cell Cycle. 2007; 6:2760–2767. [PubMed: 17986860]
20. Yamauchi T, Ishidao T, Nomura T, et al. A B-Myb complex containing clathrin and filamin is required for mitotic spindle function. EMBO J. 2008; 27:1852–1862. [PubMed: 18548008]
21. Knight AS, Notaridou M, Watson RJ. A Lin-9 complex is recruited by B-Myb to activate transcription of G2/M genes in undifferentiated embryonal carcinoma cells. Oncogene. 2009; 28:1737–1747. [PubMed: 19252525]
22. Dahl JA, Collas P. Q2ChIP, a quick and quantitative chromatin immunoprecipitation assay, unravels epigenetic dynamics of developmentally regulated genes in human carcinoma cells. Stem Cells. 2007; 25:1037–1046. [PubMed: 17272500]
23. Maya-Mendoza A, Petermann E, Gillespie DA, et al. Chk1 regulates the density of active replication origins during the vertebrate S phase. EMBO J. 2007; 26:2719–2731. [PubMed: 17491592]
24. Seiler JA, Conti C, Syed A, et al. The intra-S-phase checkpoint affects both DNA replication initiation and elongation: Single-cell and -DNA fiber analyses. Mol Cell Biol. 2007; 27:5806–5818. [PubMed: 17515603]
25. Rogakou EP, Pilch DR, Orr AH, et al. DNA double-stranded breaks induce histone H2AX phosphorylation on serine 139. J Biol Chem. 1998; 273:5858–5868. [PubMed: 9488723]
26. Alvino GM, Collingwood D, Murphy JM, et al. Replication in hydroxyurea: It's a matter of time. Mol Cell Biol. 2007; 27:6396–6406. [PubMed: 17636020]
27. Grallert B, Boye E. The multiple facets of the intra-S checkpoint. Cell Cycle. 2008; 7:2315–2320. [PubMed: 18677104]
28. Osterloh L, von Eyss B, Schmit F, et al. The human synMuv-like protein LIN-9 is required for transcription of G2/M genes and for entry into mitosis. EMBO J. 2007; 26:144–157. [PubMed: 17159899]
29. Knight AS, Notaridou M, Watson RJ. A Lin-9 complex is recruited by B-Myb to activate transcription of G(2)/M genes in undifferentiated embryonal carcinoma cells. Oncogene. 2009; 28(15):1737–47. [PubMed: 19252525]
30. Dominguez-Sola D, Ying CY, Grandori C, et al. Non-transcriptional control of DNA replication by c-Myc. Nature. 2007; 448:445–451. [PubMed: 17597761]
31. Wierstra I, Alves J. FOXM1, a typical proliferation-associated transcription factor. Biol Chem. 2007; 388:1257–1274. [PubMed: 18020943]
32. Tan Y, Raychaudhuri P, Costa RH. Chk2 mediates stabilization of the FoxM1 transcription factor to stimulate expression of DNA repair genes. Mol Cell Biol. 2007; 27:1007–1016. [PubMed: 17101782]
33. Garner-Hamrick PA, Fisher C. Antisense phosphorothioate oligonucleotides specifically down-regulate cdc25B causing S-phase delay and persistent antiproliferative effects. Int J Cancer. 1998; 76:720–728. [PubMed: 9610732]
34. Boutros R, Dozier C, Ducommun B. The when and wheres of CDC25 phosphatases. Curr Opin Cell Biol. 2006; 18:185–191. [PubMed: 16488126]
35. Costa RH. FoxM1 dances with mitosis. Nat Cell Biol. 2005; 7:108–110. [PubMed: 15689977]
36. Yim H, Erikson RL. Polo-like kinase 1 depletion induces DNA damage in early S prior to caspase activation. Mol Cell Biol. 2009; 29:2609–2621. [PubMed: 19289504]
37. Nakagoshi H, Kanei-Ishii C, Sawazaki T, et al. Transcriptional activation of the c-myc gene by the c-myb and B-myb gene products. Oncogene. 1992; 7:1233–1240. [PubMed: 1594249]
38. Watson RJ, Robinson C, Lam EW. Transcription regulation by murine B-myb is distinct from that by c-myb. Nucleic Acids Res. 1993; 21:267–272. [PubMed: 8382794]
39. Linhart C, Elkon R, Shiloh Y, et al. Deciphering transcriptional regulatory elements that encode specific cell cycle phasing by comparative genomics analysis. Cell Cycle. 2005; 4:1788–1797. [PubMed: 16294034]
40. Korver W, Schilham MW, Moerer P, et al. Uncoupling of S phase and mitosis in cardiomyocytes and hepatocytes lacking the winged-helix transcription factor Trident. Curr Biol. 1998; 8:1327–1330. [PubMed: 9843684]

41. Wang X, Kiyokawa H, Dennewitz MB, et al. The Forkhead Box m1b transcription factor is essential for hepatocyte DNA replication and mitosis during mouse liver regeneration. Proc Natl Acad Sci USA. 2002; 99:16881–16886. [PubMed: 12482952]

42. Davis AC, Wims M, Spotts GD, et al. A null c-myc mutation causes lethality before 10.5 days of gestation in homozygotes and reduced fertility in heterozygous female mice. Genes Dev. 1993; 7:671–682. [PubMed: 8458579]

43. Ma H, Samarabandu J, Devdhar RS, et al. Spatial and temporal dynamics of DNA replication sites in mammalian cells. J Cell Biol. 1998; 143:1415–1425. [PubMed: 9852140]

44. Fernandez PC, Frank SR, Wang L, et al. Genomic targets of the human c-Myc protein. Genes Dev. 2003; 17:1115–1129. [PubMed: 12695333]

Europe PMC Funders Author Manuscripts

Europe PMC Funders Author Manuscripts

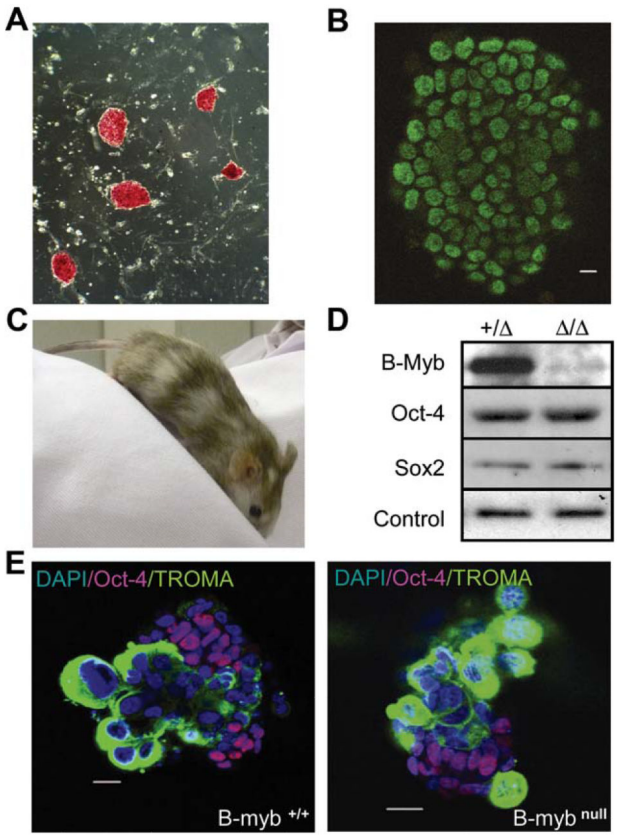

Figure 1. Characterization of *B-myb*$^{F/\Delta}$ ESCs, *B-myb*$^{\Delta/\Delta}$ ESCs and *B-myb*^{null} blastocysts.
B-*myb*$^{F/\Delta}$ ESCs stained with (**A**) alkaline phosphatase (red, ×5 objective) and (**B**) Oct-4 (green, scale bar = 10 μm). (**C**): Adult chimera generated by injection of 129/Sv *B-myb*$^{F/\Delta}$ ESCs into FVB/N blastocysts. Here is shown a mouse with 70% chimerism. Similar results were obtained for *B-myb*$^{+/\Delta}$ ESCs (data not shown). (**D**): Western blots of B-Myb, Oct-4, and Sox-2 proteins in *B-myb*$^{+/\Delta}$ and *B-myb*$^{\Delta/\Delta}$ ESCs. Histone deacetylase 1 (HDAC1) was used as a control. (**E**): Representative confocal images (middle slice) of *B-myb*$^{+/+}$ and *B-myb*^{null} blastocyst outgrowths cultured for 72 hours stained with TROMA-1 (green) and Oct-4 (red) antibodies. Scale bar = 5 μm. Abbreviations: DAPI, 4′,6-diamidino-2-phenylindole; TROMA, cytokeratin-endoA.

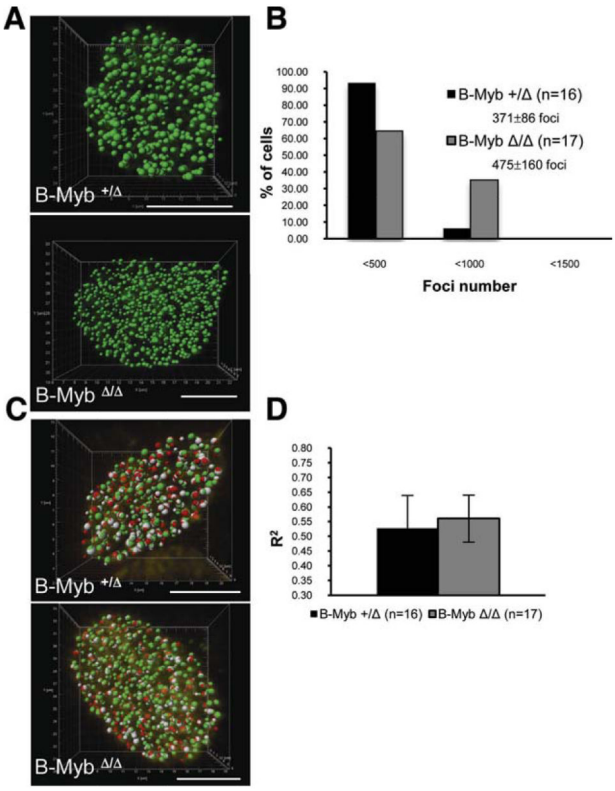

Figure 2. Replication studies in whole *B-myb*$^{+/\Delta}$ and *B-myb*$^{\Delta/\Delta}$ ESCs, 96 hours after transfection with Cre recombinase.

(**A**): Three-dimensional (3D) rendering images of BrdU-labeled replication foci (green) in ESC nuclei in early S phase: *B-myb*$^{+/\Delta}$ nucleus (top, 418 foci) and *B-myb*$^{\Delta/\Delta}$ nucleus (bottom, 767 foci). Scale bar = 5 μm. (**B**): Distribution of BrdU-labeled replication foci per cell in early S phase. Means ± SD are indicated (medians, n = 16/17, α = 0.05, p = .044, two-tailed Mann-Whitney test). (**C**): Colocalization analysis of replication factories in early S phase nuclei in *B-myb*$^{+/\Delta}$ and *B-myb*$^{\Delta/\Delta}$ ESCs pulse labeled for 20 minutes with BrdU (green) and then for 25 minutes with IdU (red). The colocalization function of Imaris was used to generate a colocalization channel. 3D spots were created and depicted as white colocalized foci: *B-myb*$^{+/\Delta}$ nucleus (top, r^2 = .57) and *B-myb*$^{\Delta/\Delta}$ nucleus (bottom, r^2 = .54). Scale bar = 5 μm. 3D image visualization (top left) and 3D image rendering (bottom left) of z-stack images from confocal microscope using Imaris software. The colocalization function of Imaris was used to generate a colocalization channel. 3D spots were created and depicted as white colocalized foci. (**D**): Average of square root of the Pearson's correlation coefficient (r^2) in early S phase of *B-myb* $^{+/\Delta}$ and *B-myb*$^{\Delta/\Delta}$ ESCs 96 hours after transfection with Cre. Pearson's correlation coefficients were generated using the colocalization function of Imaris. Means ± SD are indicated (medians, n = 16/17, α = 0.05, p = .3973, Mann-Whitney test).

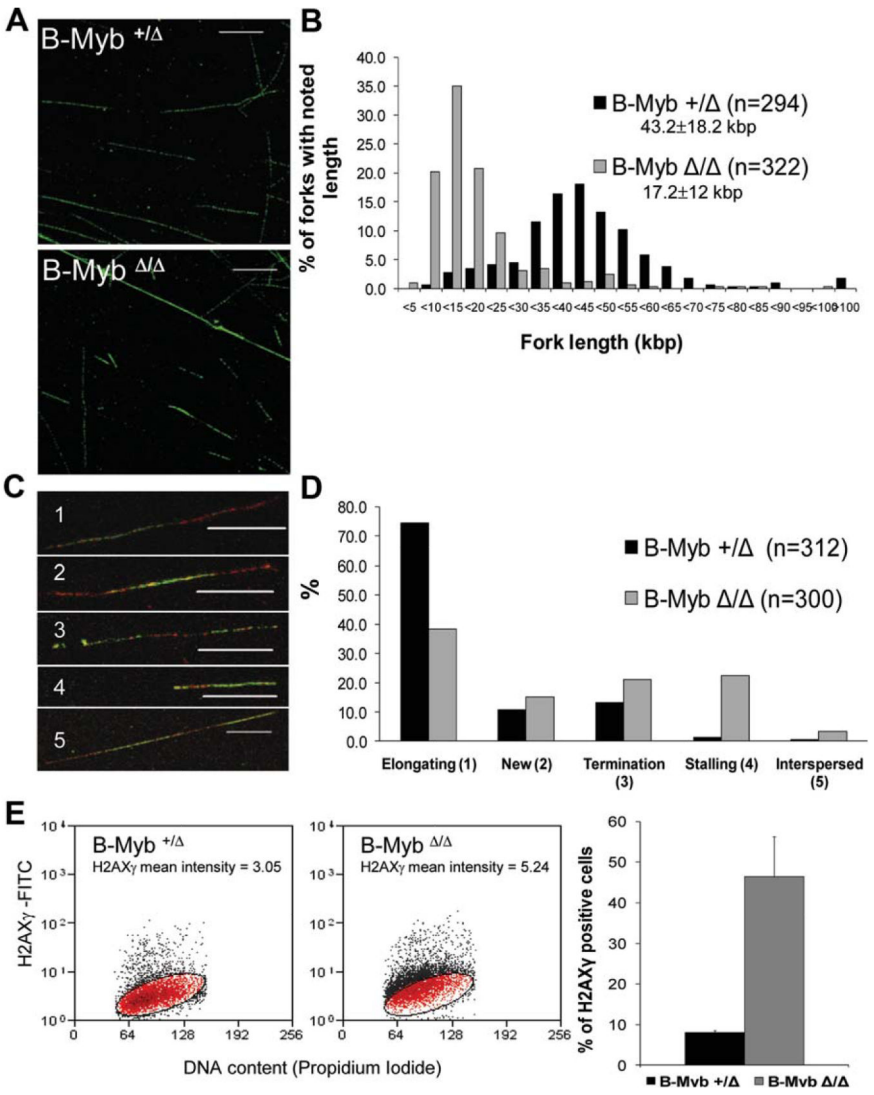

Figure 3. Replication studies on single DNA fibers comparing *B-myb*$^{+/\Delta}$ and *B-myb*$^{\Delta/\Delta}$ ESCs 96 hours after transfection.

(**A**): *B-myb*$^{+/\Delta}$ and *B-myb*$^{\Delta/\Delta}$ ESCs were pulse labeled for 20 minutes prior DNA fiber spread. Pictures show BrdU-labeled DNA fibers (green). Scale bar = 10 μm. (**B**): Frequency histogram of replication fork length. Means ± SD are indicated (means, n = 294/322, α = 0.05, p = 1.2 e −69, two-tailed unequal variance Student's t-test). Rates of fork elongation for *B-myb*$^{+/\Delta}$ and *B-myb*$^{\Delta/\Delta}$ ESCs are 1.7 ± 0.73 and 0.7 ± 0.48 kbp/minute, respectively. (**C**): Representative images of replication structures (1–5) scored after Bromodeoxyuridine (green) and Iododeoxyuridine (red) labeling. Scale bar = 10 μm. (**D**): Relative frequency of occurrence of the different replication structures (n = 300/312, α = 0.05, p = 3.19 e −22, two-tailed χ^2 contingency test). (**E**): Bivariant flow cytometric analysis of H2AXγ and DNA content. Cells negative for H2AXγ are represented in red within the ellipse and H2AXγ means intensity are indicated (left). Mean percentages of H2AXγ positive cells ± SD are indicated in the histogram (right; n = 3, α = 0.05, p = .021, two-tailed unequal variance Student's t-test). Abbreviation: FITC, Fluorescein Isothiocyanate.

Europe PMC Funders Author Manuscripts

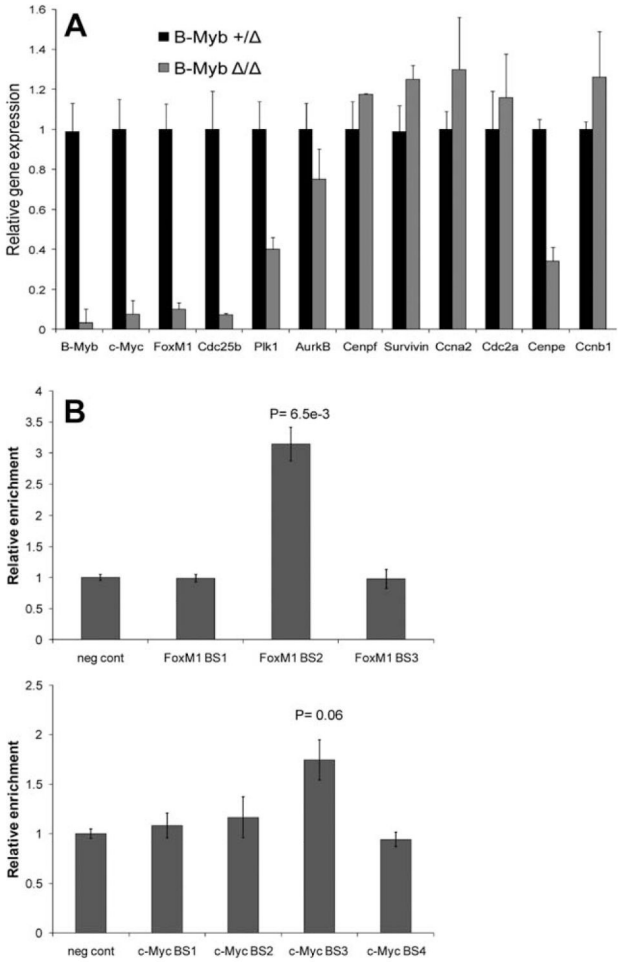

Figure 4. B-Myb regulates *c-Myc* and *FoxM1* expression in ESCs.

(**A**): Gene expression changes consequent to the ablation of B-Myb measured by Quantitative Reverse Transcriptase-PCR (qRT-PCR) of cell cycle genes in *B-myb*$^{+/\Delta}$ and *B-myb*$^{\Delta/\Delta}$ ESCs, 48 hours after transfection with Cre recombinase. (**B**): Representative X-ChIP on TL1 ESCs using B-Myb antibody. Enrichment fold was determined against negative control region. Graphs illustrate level of enrichment for each binding site identified for *FoxM1* gene (upper) and *c-myc* gene (lower). *p* values obtained by two-tailed equal variance Student's *t*-test were calculated for enriched binding sites FoxM1 BS2 ($n = 5$, $\alpha = 0.05$, $p = 6.5\ e\ {-3}$) and c-Myc BS3 ($n = 5$, $\alpha = 0.05$, $p = .06$).

Europe PMC Funders Author Manuscripts

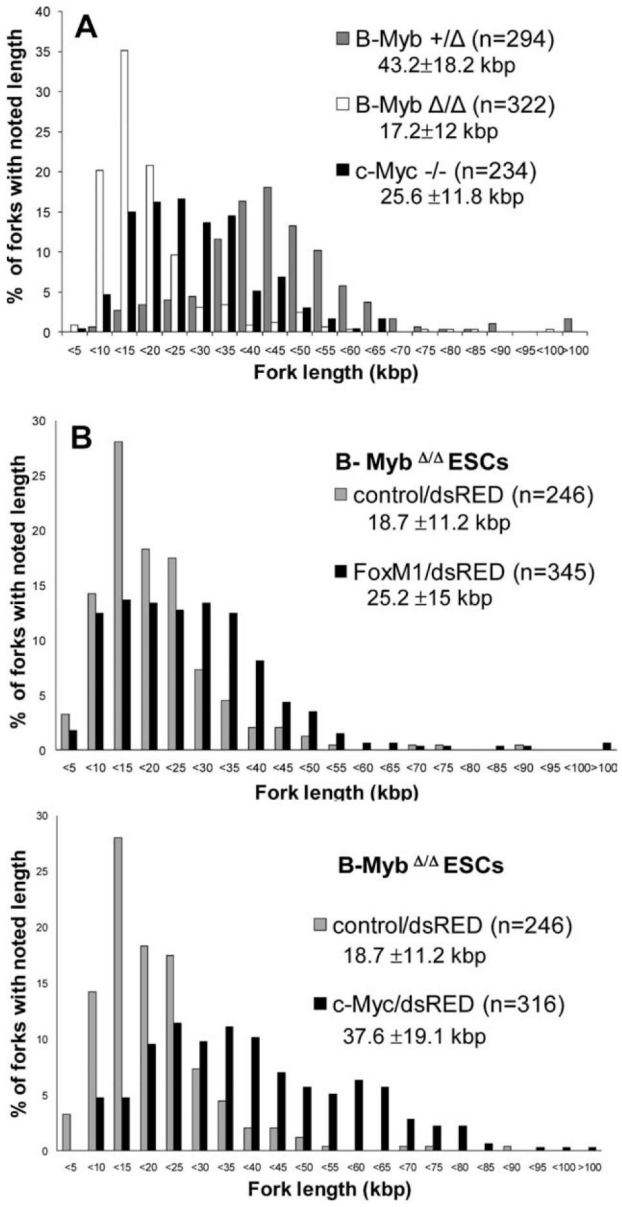

Figure 5. Replication studies on single DNA fibers of *c-myc*$^{-/-}$ ESCs and of *B-myb*$^{\Delta/\Delta}$ ESCs rescued with c-Myc/dsRed or FoxM1/dsRed.

(**A**): *c-myc*$^{-/-}$ ESCs were pulse labeled for 25 minutes prior DNA fiber spread. Frequency histogram of replication fork length. Means ± SD are indicated (means, n = 294/234/322, α = 0.05, p = 2.15 e −35 between *B-myb*$^{+/\Delta}$ and *c-myc*$^{-/-}$ and p = 1.34 e −15 between *B-myb*$^{\Delta/\Delta}$ and *c-myc*$^{-/-}$, two-tailed unequal variance Student's t-test). Rates of fork elongation for *B-myb*$^{+/\Delta}$, *B-myb*$^{\Delta/\Delta}$, and *c-myc*$^{-/-}$ ESCs are 1.7 ± 0.73, 0.7 ± 0.48, and 1.0 ± 0.47 kbp/minute, respectively. (**B**): *B-myb*$^{\Delta/\Delta}$ ESCs 72 hours after transfection with control/dsRED, c-Myc/dsRED, or FoxM1/dsRED were pulse labeled for 25 minutes prior DNA fiber spread. Frequency histograms of replication fork length for *B-myb*$^{\Delta/\Delta}$ + c-Myc/dsRED (lower graph) and for *B-myb*$^{\Delta/\Delta}$ ± FoxM1/dsRED (upper graph). Means ± SD are indicated (means, n = 246/316/265, α = 0.05, p = 5.74 e −41 between control/dsRED and c-Myc/dsRED and p

= 2.46 e −9 between control/dsRED and FoxM1/dsRED, two-tailed unequal variance Student's *t*-test). Rates of fork elongation for *B-myb*$^{\Delta/\Delta}$ ESCs plus control/dsRED, c-Myc/dsRED, or FoxM1/dsRED are 0.7 ± 0.45, 1.5 ± 0.76, and 1.0 ± 0.64 kbp/minute, respectively.

Europe PMC Funders Author Manuscripts

Europe PMC Funders Author Manuscripts

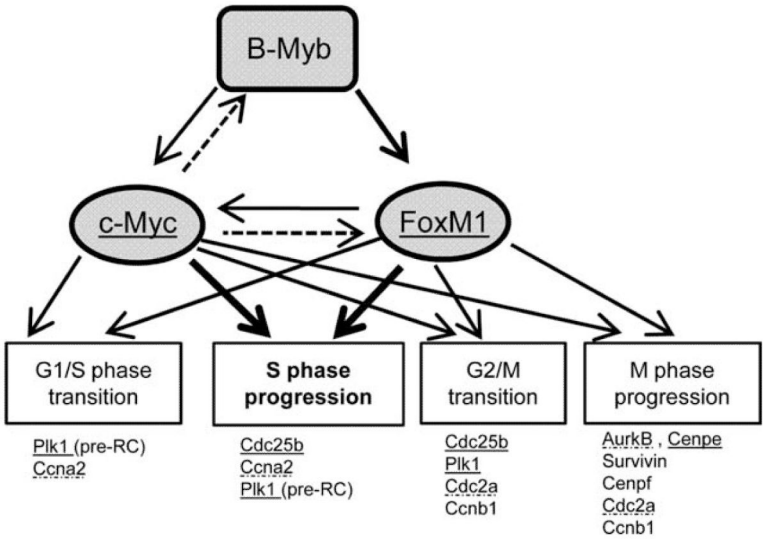

Figure 6. Model illustrating the role of B-Myb in cell cycle gene regulation.

We propose that B-Myb regulates c-Myc and FoxM1, which in turn regulate genes involved at different stages of the cell cycle. Established interactions are shown with full arrows, whereas hypothetical ones are depicted as dashed arrows. It is indicated if specific gene expression was downregulated 48 hours after transfection with Cre (underlined), 11 days after transfection (dashed underlined) and not affected (not underlined) on B-Myb ablation.